Microgrooving and microthreading tools for fabricating curvilinear features

D.P. Adams[a,*], M.J. Vasile[b], A.S.M. Krishnan[b]

[a]*Sandia National Laboratories, Albuquerque, NM, USA*, [b]*Louisiana Tech University, Ruston, LA, USA*

Abstract

This paper presents techniques for fabricating microscopic, curvilinear features in a variety of workpiece materials. Microgrooving and microthreading tools with cutting widths as small as 13 μm are made by focused ion beam sputtering and used for ultraprecision machining. Tool fabrication involves directing a 20 keV gallium beam at polished cylindrical punches made of cobalt M42 high-speed steel or C2 tungsten carbide to create a number of critically aligned facets. Sputtering produces rake facets of desired angle and cutting edges having radii of curvature equal to 0.4 μm. Clearance for minimizing frictional drag of a tool results from a particular ion beam/target geometry that accounts for the sputter yield dependence on incidence angle. It is believed that geometrically specific cutting tools of this dimension have not been made previously. Numerically controlled, ultraprecision machining with microgrooving tools results in a close match between tool width and feature size. Microtools are used to machine 13-μm wide, 4-μm deep, helical grooves in polymethyl methacrylate and 6061 Al cylindrical workpieces. Microgrooving tools are also used to fabricate sinusoidal cross-sectional features in planar metal samples. © 2000 Elsevier Science Inc. All rights reserved.

Keywords: Microtools; Micromachining; Ultraprecision

1. Introduction

Alternative fabrication techniques are currently being explored to meet the manufacturing requirements of microsystems [1]. Although many microcomponents and microelectromechanical devices have been demonstrated in recent years, most fabrication has involved inherently planar techniques, such as X-ray or optical lithography. Features are defined in polished substrates or thin film layers by exposure of a resist (using a mask) and etching. However, there is a need to fabricate more complex shaped features in a variety of ceramics, metals, and polymers. For example, nonprismatic features and nonplanar workpieces are essential for a variety of devices. These include microfluidic sensors [2], microinductors [3], and microactuators [4].

Recently, several groups have demonstrated techniques that fabricate curvilinear features. These include microcontact printing [5], which applies a two-dimensional (2-D) lithographic master to a substrate such as a cylinder, and laser chemical vapor deposition [6,7], which involves direct writing of materials via pyrolysis or photodecomposition of precursor gases. Other inherently planar techniques, such as Lithographie-Galvanoformung-Abfromung (LIGA) [8] are also being adapted to produce overhangs and curved features [9–13]. Nevertheless, additional capabilities are required, because many of the previously mentioned techniques are limited in dimensionality, material complexity, or microstructure control.

Often the combination of different microfabrication techniques enhances process applicability [9,14,15]. In the present work, focused ion beam sputtering is combined with ultraprecision machining. Focused ion beam (FIB) sputtering is used to make microcutting tools intended for mechanical machining of polymer and metal alloy workpieces. FIB sputtering is attractive for fabricating micron-size tools or instruments, because this technique can precisely remove or add material [16,17]. Commercial focused ion beam systems are quite powerful, providing 10-nA currents, 10-nm spot sizes, and 10-nm pixel spacings. Most importantly, focused ion beam sputtering can be used to create and align a number of nonplanar features, such as facets required on microshaping tools. Several studies demonstrate FIB-sput-

————
* Corresponding author. Tel.: +505-844-8317; fax: +505-844-2754.
E-mail: dpadams@sandia.gov (D.P. Adams).

tered microgears, microwrenches, microscalpels, and nanoindenters [18–20]. Ultraprecision machining is beneficial for microfabrication because of its accuracy and speed. The intent of current work is to fabricate micron size features over centimeter length scales in a reasonable time. This is potentially achievable, because commercial ultraprecision machines have a 5-nm resolution. Furthermore, it is expected that tools having $\sim$ 25 μm diameters are robust and reproducibly define microscopic features. Recent work shows that ground metal microend mill tools having cutting diameters of $\sim$ 50–100 μm successfully machine small grooves in acrylic polymer [21] and stainless steel workpieces [22]. Additional studies demonstrate that $\sim$ 25 μm diameter, FIB-fabricated micro-end mills machine trenches in polymethyl methacrylate (PMMA) and metal workpieces [23–26]. Material has been mechanically removed from metal alloy workpieces at a rate of 2×10^4 μm^3/s for over 1 h [26]. In comparison, typical ion beam sputter removal rates are $\sim$ 0.1–20 μm^3/s using commercial FIB systems [27–29]. In the present work, focused ion beam sputtering is combined with ultraprecision machining to create complex features in a variety of materials. This includes micromachining approximately 15–100 μm wide, curvilinear features in planar and cylindrical workpieces.

2. Experimental systems and analysis techniques

Microgrooving and microthreading tools are fabricated in a focused ion beam system designed and built at AT&T Bell Laboratories, as described in detail elsewhere [30]. A liquid metal ion gun produces a 20-keV beam of Ga$^+$ ions with a Gaussian intensity distribution and a full-width at half-maximum diameter of 0.4 μm on target. Currents are typically 2 nA in a Faraday cup, giving a current density of $\sim$ 1.5 A/cm^2. In practice, an operator outlines a desired shape for removal on a secondary electron image of the target, and an octapole deflection system steers the ion beam to designated areas with submicron resolution. Between sputter removal steps, a stage positions tools with 1 μm accuracy. This stage also provides for sample rotation [19] with a minimum step size of 0.37° per pulse, which is a critical element of tool fabrication. The Ga$^+$ source chamber is ion pumped and maintains a pressure of 10^{-9} Torr. The target chamber has an oil diffusion pump and pressures of 10^{-8} Torr during sputtering. A small aperture separates the two chambers for differential pumping.

Tool blanks are purchased from National Jet, Inc. and are made of cobalt M42 high-speed steel or C2 micrograin tungsten carbide. Tool shanks have a diameter of 1.02 mm and are brazed into a centerless ground mandrel. Tool mandrels are either 2.3 mm or 3.175 mm in diameter. One end of each tool is tapered by diamond grinding and polished; this end has a diameter of approximately 25 μm and is cylindrical over a length of 25 μm.

Ultraprecision machining with FIB-fabricated microtools

involves two instruments: a modified National Jet 7M instrument (a joint program involving Louisiana Tech University, National Jet Company and Dover Instruments) for planing operations and a Precitech Optimum 2000 high-precision lathe. The National Jet instrument has a 1,500 kg granite machine base for vibrational and thermal stability, and all axes have air bearings. The x and y motions of the worktable employ laser interferometry with a commanded resolution of 1.25 nm, and the z motion has linear encoder positional control with a resolution of 20 nm and a vertical travel range of 150 mm. This instrument is adapted for microplaning operations with no tool rotation. Rotation is arrested by locking the spindle at a reference position. The Precitech lathe operates with both the x- and z-axis drive mechanisms mounted on a granite platform lapped co-planar to 1.3 μm and isolated from the machine frame to prevent unwanted vibrations. Identical fully constrained, dovetail-type air-bearing slides provide smooth motion for the two axes with less than 0.25 μm deviation per 102 mm of motion. The total length of travel is 191 mm and the maximum slide speed is 1,000 mm/min. The two slides are oriented perpendicular to within 2 arc-s. Linear laser holographic scales and read-head assemblies provide stable positional feedback for both axes with 8.6 nm resolution. The spindle is supported by fully preloaded, high stiffness air bearings and is driven by an integrally mounted brushless DC motor and encoder with a range from 0 to 5,000 rpm. For both instruments, registry involves probing for electrical continuity between tool and workpiece as the tool is stepped toward the sample. To "touch-off" accurately, nonconductive workpieces are coated with a 20-nm thick, conductive layer of Au/Pt before mounting. Cutting operations, and registry, are also monitored with an optical microscope and a charged coupled-device (CCD) camera. Water continuously flushes workpieces during ultraprecision machining. After machining, workpieces are rinsed with isopropyl alcohol. However, in this study, burrs are not removed by mechanical or electrochemical polishing.

Fabricated microtools and certain micromachined workpieces are analyzed by scanning electron microscopy (SEM). An over-all accuracy of 95% or better is estimated for dimensions measured by SEM. Tool dimensions, tool edge radius of curvature, taper angles, and rake angles are investigated using an Amray 1830 scanning electron microscope. This microscope is calibrated to a NIST SRM 2090 standard in the 100 μm range and shows a -2.4 to -2.6% error when using a fixed working distance (i.e., bottom of pole piece to sample surface). In addition, a calibrated JEOL 6300 V scanning electron microscope is used to measure widths of grooves machined in cylindrical workpieces. This instrument is calibrated to a NIST/NBS standard (reference # 484 c) and shows less than a 2% error for different working distances. The widths of grooves machined in cylindrical workpieces are determined by viewing feature cross section. Images that show perspective views are not used for measurement.

A calibrated WYKO (RST+) white light optical interferometric roughness step tester determines the widths of grooves machined into planar workpieces and the surface finish laterally and longitudinally along the bottom surface of micromachined grooves. The step height standard is a 23.33 μm metal film (VLSI Standards, Inc.). The phase shift interference resolution of the RST+ is 0.3 nm.

3. Focused ion beam fabrication of microtools

Microgrooving and microthreading tools have designs similar to conventional lathe cutting tools; however, cutting edge dimensions are in the ~10–30 micron range. Each microtool is fabricated from a polished blank to have sharp cutting edges, clearance behind cutting edges, and rake features. This is achieved by sputtering a number of strategically placed facets on cylindrical or conical sections at the end of a tool blank. In general, the tool rotation/sputter sequence and the location of facets are critical for defining tool characteristics (rake, etc.).

The first step of fabricating all microgrooving and microthreading tools involves shortening polished blanks. A smooth facet is sputtered at the tool end, as shown in Fig. 1. After sputtering, the end facet normal is nearly aligned with the tool axis.

Next, two facets are created on opposite sides of a tool (step 2). This sputter step determines the cutting width, tool cross section, and, hence, the intended cross-sectional shape of a micromachined groove. For example, ion milling two nearly parallel facets creates a tool with a rectangular cutting shape. Alternatively, a threading tool that cuts trapezoidal cross-sectional grooves is fabricated by ion milling two nonparallel facets. Sputtering side facets with the geometry shown is critical for establishing taper. Taper provides clearance behind side facet cutting edges (defined in step 3), thus minimizing contact with workpieces and reducing frictional drag on a tool. During sputtering, each side facet forms a natural taper angle of ~5–10° with respect to the ion beam direction. This results from the maximum sputter yield at incidence angles between 75 and 85° with respect to the surface normal [27,31]. Identical taper angles are created, symmetric about the tool end, when using the geometry shown in step 2. Note, a different taper angle behind cutting edges can be established by rotating the sample stage/tool before sputtering of individual side facets.

After creating side facets, the focused ion beam is used to define rake features that clear chips during ultraprecision machining. First, each tool is rotated −90° to the orientation shown in Fig. 1, step 3. This orients one side facet away from the ion source and places the second side facet such that it nearly faces the source. A triangular projected area is then ion milled on one side of a tool to define a desired back rake angle. The FIB system can accurately define this angle with a resolution of 0.25°. In this study, microgrooving tools are made with a back rake angle between 7 and 10°,
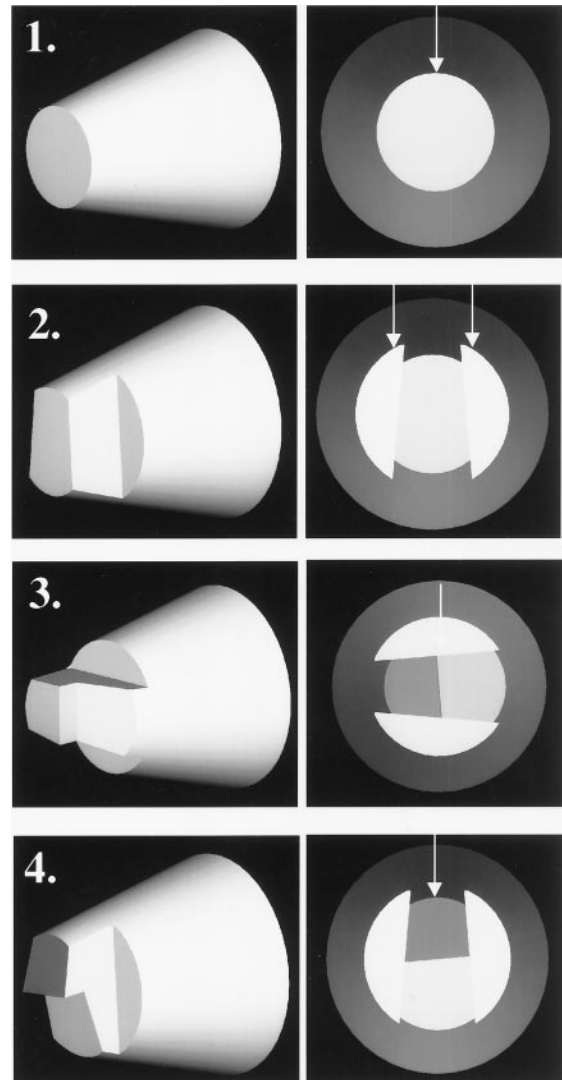

Fig. 1. Procedure for making a microgrooving tool using focused ion beam sputtering. Arrows indicate the direction of ion beam impingement. The tool is rotated −90° between steps 2 and 3 and +90° between steps 3 and 4. Images in left column show tilted view of model tool. Complementary images in right column are end-on views.

referenced to the tool axis. Microthreading tools have a 0° back rake angle for increased rigidity. FIB sputtering is also used during this step to set the rake facet length, typically 10–20 μm. Note, a natural taper angle of ~5–10° with respect to the ion beam direction accompanies rake feature definition, independent of the back rake angle chosen. This taper can be used to establish side rake, displayed in an end-on view of a model tool (Fig. 1, step 3). The side rake angle can be changed or eliminated; that is, forced to 0°, by proper rotation of the stage/tool before ion milling this facet.

A sharp cutting edge having clearance is created at the microtool end as a final step of fabrication. Tools are first rotated to their original orientation with respect to the ion beam, and the length is reduced approximately 3 μm by sputtering. This creates an end facet (shaded in Fig. 1, step 4) that intersects the rake facet at a well-defined, sharp edge.

Measurements from SEM show this edge has a radius of curvature (R_c) of 0.4 μm or less. Radii are measured by viewing parallel to the cutting edge. Previous work demonstrates that the ion source/target geometry shown produces sharper edges on the side of facets furthest from the ion source.[23,24] The facet edge closest to the ion source is rounded because of the part of the Gaussian beam intensity that extends outside the defined pattern boundary. A sharp cutting edge is produced on the far side, because the ion beam has a truncated intensity distribution attributable to shadowing by the tool facet. In addition to creating a sharp edge for cutting, this ion-milling geometry establishes clearance. A taper angle of ~5–10° behind the end-facet cutting edge prevents unnecessary contact with workpieces. It is important to use an identical tool orientation for sputter steps 2 and 4 to orient the taper of side facets properly with the taper of an end facet. This determines the direction of workpiece motion during ultraprecision machining.

The microtool fabrication technique outlined in Fig. 1 is one variant that can be modified to make tools with different cross-sectional shapes, including semicircular or trapezoidal. Examples of two different FIB-fabricated tools are shown in Figs. 2 and 3. A microgrooving tool identical to the model is presented in Fig. 2. This is referred to as a microgrooving tool because of the application described later in this paper. It cuts a near rectangular cross-sectional groove into planar or nonplanar workpieces. This tungsten carbide tool has a cutting edge width of 18 μm and clearance behind all cutting edges. Fig. 2b shows a 7° back rake facet that extends 8 μm, designed to deflect chips away from the cutting edge and workpiece surface. This tool has side rake, as demonstrated in Fig. 2c. Microthreading tools are also made by ion sputtering, as shown in Fig. 3. These tools are similar to microgrooving tools in size; however, they have a trapezoidal cross section and 0° rake angles. The image in Fig. 3b shows the three cutting edges of a microthreading tool, similar to a stub-threading tool. The side facet cutting edges are oriented 90° apart, and the leading edge of the tool is 15 μm wide. The taper behind cutting edges is displayed in a secondary electron micrograph of the tool end, Fig. 3c.

The small but detectable roughness of cutting facets is due to ion beam sputtering. Most likely, the compositional inhomogeneity of a tool affects the smoothness. Track marks can develop along facets during sputtering because of shadowing by second phase particles (or other compositional variations) within a tool. For example, cobalt is present in C2-grade tungsten carbide and has a different sputter yield as compared with the matrix. Fabricated microtools are polycrystalline with grains oriented in different directions. Track marks and compositional variations within C2 tungsten carbide are seen in Fig. 2.b and c. In these micrographs, regions that have a low electron yield appear dark. Energy-dispersive X-ray spectroscopy reveals that the low yield features are Co-rich and C-rich regions. We expect that sharper tool cutting edges can be achieved by
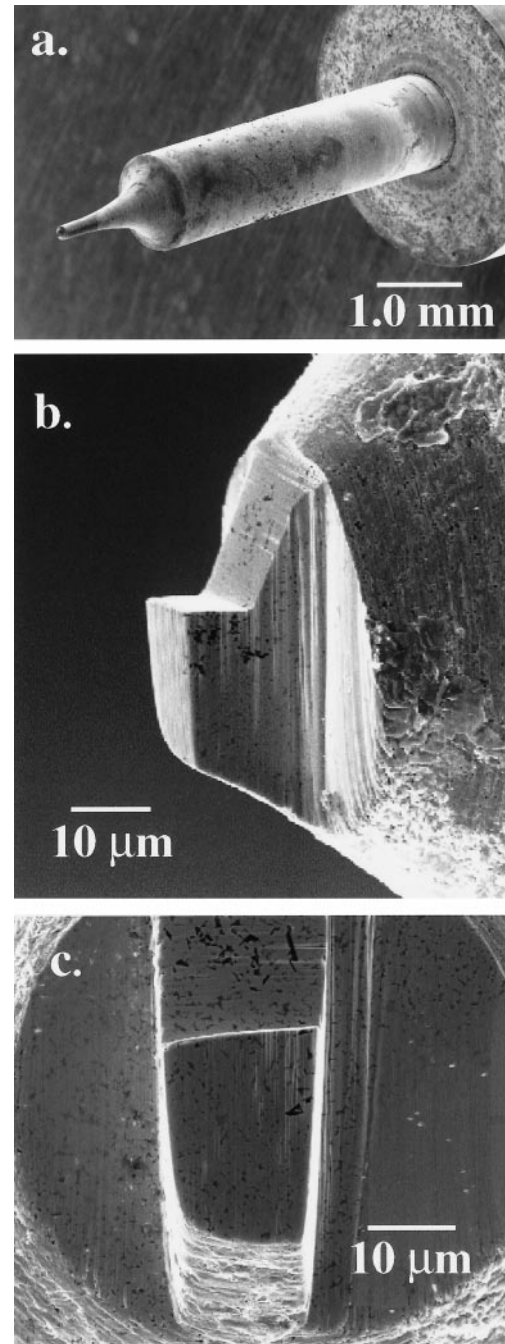

Fig. 2. Tungsten carbide microgrooving tool fabricated by focused ion beam sputtering. Tool has a near rectangular cross section with an 18-μm wide tool end cutting edge. Images show different perspectives of the microtool but do not correlate with a tool's orientations with respect to the focused ion beam.

focused ion beam sputtering of other tool materials. Single crystal materials (e.g., diamond) should exhibit minimal variation in sputter yield from point to point because of compositional uniformity.

Microtools are fabricated in 4–5 h, depending on tool dimensions, design, and material composition. Fabrication time is determined principally by the amount of material removed. Hence, a smaller tool requires less time for sput-
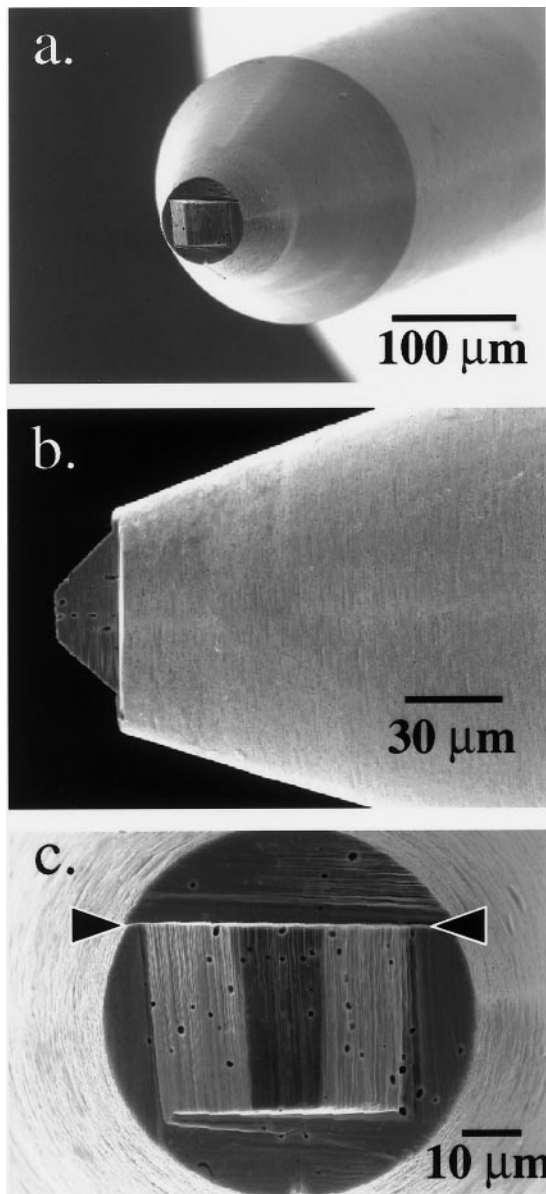
Fig. 3. High-speed steel microthreading tool fabricated by focused ion beam sputtering. Image 3.b. is a view normal to the cutting face showing a trapezoidal cross section. Image 3.c. is a view parallel to the tool axis, indicating clearance taper behind cutting edges. Cutting edges are indicated in 3.c. with arrowheads.

tering. The fabrication time varies with tool composition (high-speed steel or tungsten carbide), because sputter rate is a function of target mass. The average sputter rate for C2 carbide is known from a previous study [26] to be 0.76 $\mu m^3/s$ when using a beam current of 2.8 nA and a beam energy of 20 keV.

4. Ultraprecision machining

This section describes a number of tests that demonstrate the performance of focused ion beam fabricated microtools.

Tests involve machining increasingly complex features in polymer and metal workpieces. First, microplaning and micrgrooving of flat workpieces are described. These investigations evaluate control of feature width and surface roughness for different machining parameters. Next, micro-machining of curvilinear features is examined. Predetermined curved shapes are cut into planar workpieces using microgrooving tools and a lathe. At the end of the discussion, machining of cylindrical workpieces is presented.

4.1. Machining of planar workpieces

4.1.1. Machining linear grooves

Microtools are first tested by planing parallel grooves in flat workpieces using the National Jet apparatus. The setup involves rigidly fixing a microgrooving tool in a collet and aligning the tool-end cutting edge perpendicular to the direction of workpiece motion. Orientation of the cutting edge with respect to the travel direction is established by closed-circuit, optical microscopic location of an alignment scribe mark on the tool mandrel. Three FIB-fabricated, high-speed steel, microgrooving tools are tested. As listed in Table 1, each microtool has a cutting edge R_c equal to 0.4 μm, similar cutting edge widths, and back rake angles. These similarities allow for a meaningful comparison of tool performance and machined feature quality. A portion of the results is presented in Tables 1 and 2. The first table highlights experiments with three workpiece materials: PMMA, 6061 aluminum, and brass. For each material, ten depths per pass are tested between 0.5–5.0 μm. Data in Table 1 represent experiments involving a single feed rate of 90 $\mu m/s$. In general, groove widths closely match the targeted dimension (actual cutting edge width). Groove widths are measured with optical interferometry by probing numerous sites along a given groove; the standard deviation taken from these measurements is also listed in Table 1, column 7. Certain machining parameters provide a close match of feature dimension and tool width. There seems to be a closer matching of groove widths to tool width at smaller depths/ pass, particularly for metal workpieces. Table 2 also suggests a better matching of tool width and feature width at smaller depths/pass. Table 2 lists results from ultraprecision machining of brass at three feed rates and four depths/pass. For each test listed, a tool makes two total passes as compared with a single pass for experiments listed in Table 1.

The bottom of micromachined grooves exhibit small surface roughness. Roughness values listed in the tables are averages taken longitudinally from three areas on 1-mm long grooves. Areas measured by optical interferometry are 100 μm long. Analysis reveals groove roughnesses (R_a) of approximately 0.10–0.60 μm. PMMA shows a range of surface roughness values between 0.12 and 0.60 μm. 6061 aluminum exhibits roughness between 0.11 and 0.25 μm, and brass has R_as between 0.17 and 0.29 μm. In addition to feature width and roughness control, microgrooving tools show good performance over time. Only one planing test

Table 1
Results from single-pass planing tests for one feed rate (90 μm/s). Tool material code: HSS = M42 cobalt high speed steel

Tool #, tool material	Tool width (μm)	Tool edge R_c (μm)	Back rake angle (deg)	Workpiece material	Depth per pass (μm)	Groove width, mean [SD] (μm)	Groove roughness, R_a (μm)
2, HSS	15.5	0.4	8.1	PMMA	2.0	15.5 [1.4]	0.30
,,	,,	,,	,,	,,	3.0	18.1 [2.4]	0.30
,,	,,	,,	,,	,,	4.0	15.3 [1.4]	0.40
,,	,,	,,	,,	,,	5.0	16.7 [0.1]	0.60
3, HSS	19.3	0.4	9.5	A1 6061	2.0	19.2 [0.8]	0.12
,,	,,	,,	,,	,,	3.0	19.7 [0.8]	0.19
,,	,,	,,	,,	,,	4.0	21.6 [0.1]	0.24
,,	,,	,,	,,	,,	5.0	22.6 [0.9]	0.22
4, HSS	16.7	0.4	9.3	Brass	2.0	17.6 [1.6]	0.29
,,	,,	,,	,,	,,	3.0	18.5 [1.6]	0.25
,,	,,	,,	,,	,,	4.0	19.9 [1.6]	0.23
,,	,,	,,	,,	,,	5.0	18.5 [0.8]	0.22

resulted in significant tool wear, leading to fracture. This was caused by rotational misalignment of a tool >5° such that a portion of a side facet contacted the wall of a micromachined feature. In this case, fracture occurred after machining 0.0014 mm^3 of 6061 Al alloy.

4.1.2. Machining concentric rings

Additional tests of microgrooving tools involve lathe machining of curved features in planar workpieces. A lathe is adapted by vacuum clamping a polished workpiece at the end of the spindle. A microtool is then aligned perpendicular to the workpiece surface so that the tool axis is parallel with the axis of rotation, as shown in Fig. 4. Cutting edges and clearance tapers determine the proper tool orientation for lathe machining, and alignment is set using a mark scribed on tool mandrels. Initial experiments involve cutting concentric rings, as shown in Fig. 5. Four concentric rings are cut into a planar aluminum workpiece using a depth per pass equal to 2 μm and a feed rate of 8 μm/s. The cutting speed is determined by the distance from the center of the rings and varies from 3,611–10,205 μm/s. The inner concentric ring is cut to a

depth of 2 μm, and the outer three are 10-μm deep. Depth is controlled by accurately registering the tool with the workpiece surface and then stepping into the bulk with a resolution of 8.6 nm. Optical interferometry shows that the average groove width, 30.7 μm, is similar to the microtool cutting width, 30.4 μm. Also, the WYKO instrument indicates the roughness (R_a) of the bottom of aluminum channels is small, 0.14–0.25 μm. Smaller surface roughness results at higher cutting speeds.

Lathe machining is also used to fabricate curvilinear features in planar samples. Specifically, microgrooving tools machine concentric rings having predetermined cross-sectional shapes. This is accomplished by coordinating the axial and lateral feed rates. A microtool is rotated slightly (compared with the orientation shown in Fig. 4), so that the effective cutting width is reduced. Fig. 6 shows an example of a curved shape machined in aluminum: two concentric rings are created having a sinusoidal cross section. A single crest is located at the original height of the workpiece surface surrounded by two concentric troughs, each 10 μm deep. Each ring is created by numerous passes to establish a smoothly varying curved surface. Using this technique, a

Table 2
Results from planing brass at different feed rates and depths/pass. A single tool is used having a cutting edge radius of curvature equal to 0.4 μm and a black rake angle equal to 9.3°. Tool material code: HSS = M42 cobalt high speed steel

Tool #, tool material	Tool width (μm)	Depth per pass (μm)	Groove depth (μm)	Feed rate (μm/s)	Groove width, mean [SD] (μm)	Groove roughness, R_a (μm)
4, HSS	16.7	1.5	3.0	60	16.8 [0.9]	0.28
,,	,,	,,	3.0	90	18.5 [0.8]	0.28
,,	,,	,,	3.0	120	16.7 [0.1]	0.18
,,	,,	2.5	5.0	60	19.4 [0.1]	0.29
,,	,,	,,	5.0	90	19.0 [0.8]	0.23
,,	,,	,,	5.0	120	18.5 [2.1]	0.17
,,	,,	3.5	7.0	60	19.4 [2.6]	0.22
,,	,,	,,	7.0	90	19.4 [1.4]	0.19
,,	,,	,,	7.0	120	19.9 [0.8]	0.21
,,	,,	4.5	9.0	60	19.9 [0.8]	0.21
,,	,,	,,	9.0	90	21.3 [1.6]	0.26
,,	,,	,,	9.0	120	19.9 [1.6]	0.22
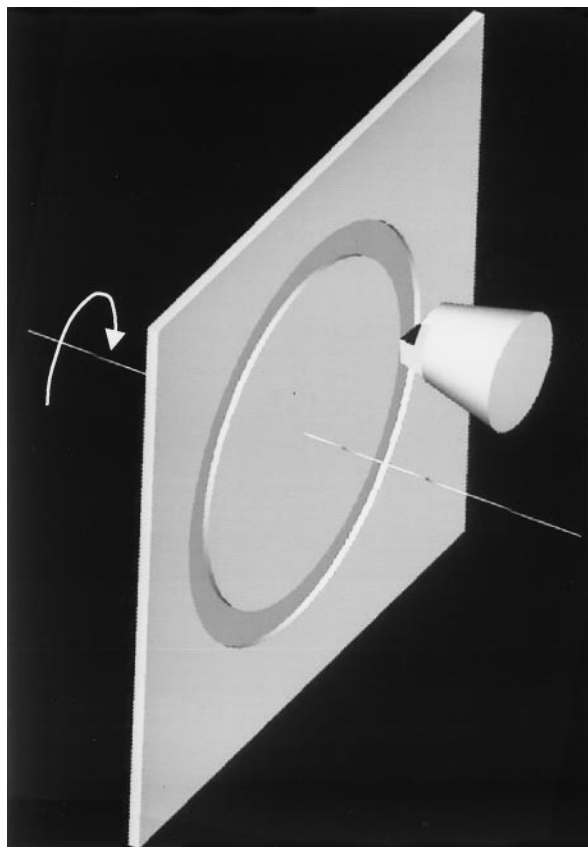
Fig. 4. Lathe setup for micromachining concentric grooves in planar workpieces.
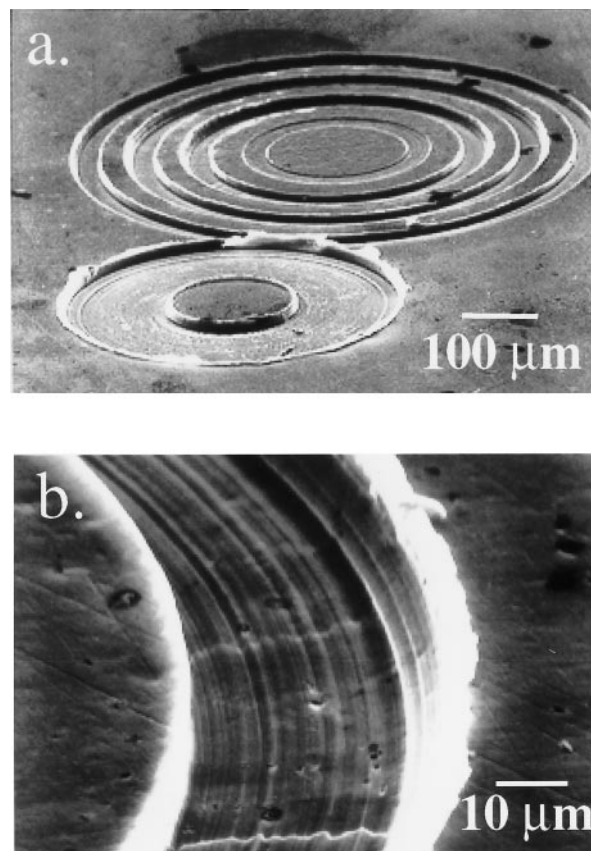

Fig. 5. Scanning electron micrographs of concentric circular grooves machined in 6061 aluminum alloy using a microgrooving tool. Also shown in (a.) is a micromachined annulus. Micrograph (b.) displays a high- magnification view of a single groove.

number of concentric rings similar to those shown in Fig. 6 are made. The minimum pitch achieved is 62.5 μm using a tool that is 30.4-μm wide. For these experiments, the spindle speed is 300 rpm, making the maximum cutting speed equal to 20,000 μm/s.

4.2. Machining of cylindrical workpieces

FIB-fabricated microgrooving tools are used to machine helical grooves in cylindrical workpieces as another test of ultraprecision machining and microtool capabilities. A polished, cylindrical workpiece is mounted into a pin vice concentric with the lathe axis of rotation, and a tool holder post is arranged perpendicular. The workpiece is first polished to run true on the lathe, using a diamond bit; this establishes a workpiece surface finish of approximately 1-μm (rms) or better. Afterward, a FIB-fabricated microtool is loaded and aligned with its axis perpendicular to the workpiece axis. Using a scribe mark on the mandrel for alignment, the tool is then rotated to an orientation such that the tool-end cutting edge is nearly parallel to the workpiece axis. An alignment accuracy of tool cutting edges to better than 0.5° ensures minimal contact of side facets with the groove wall. The microtool is then stepped toward the rotating workpiece and registered. Once the workpiece is

contacted, the tool is driven into the workpiece to a targeted groove depth, and linear motion is initiated.

Using this technique, microgrooving tools cut helical grooves into cylindrical samples made of 6061-T6 aluminum. Fig. 7 shows a portion of a 13.2-μm wide, 4-μm deep groove having a total length of 200 mm. The pitch between successive passes is 100 μm and is set by the relative rotation rate and the axial feed rate. A change in pitch can be achieved by simply increasing/decreasing these rates. Electron microscopy demonstrates a close matching of tool size and micromachined feature width. Measurements show that the groove width is approximately the same as the cutting edge width, 13.0 μm, over the length of the feature. In addition, high-magnification images, such as that shown in Fig. 7.b, demonstrate close matching of tool shape and feature cross section. SEM analysis of the micromachined groove bottom shows a 6° taper with respect to the cylinder axis. This is identical to the angle of the tool-end cutting edge.

A precise matching of tool shape and groove cross section also results from machining polymeric cylindrical workpieces. Fig. 8 shows portions of a groove cut in 1.38-mm diameter PMMA. The pitch is 50 μm, and the total groove length is 420 mm. The total time to cut PMMA is approximately 30 s. SEM measurements show that the micromachined groove is consis-
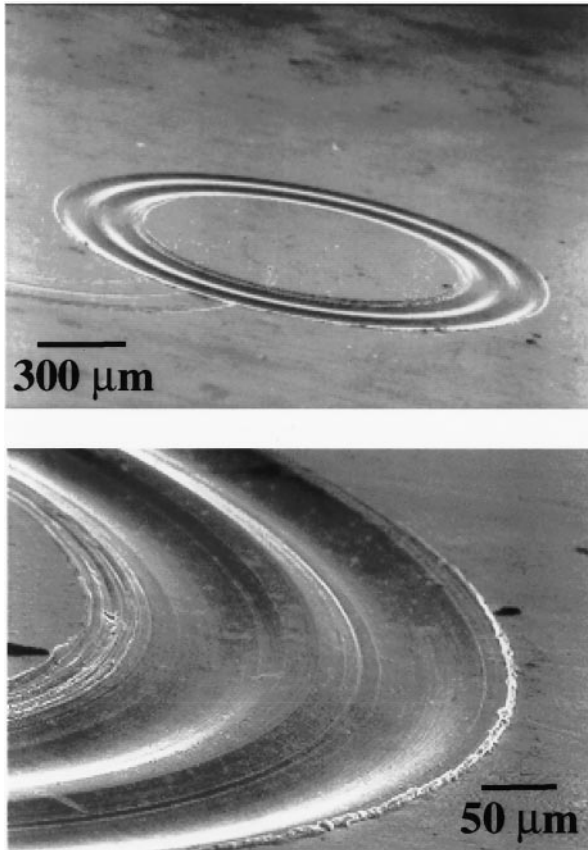
Fig. 6. Scanning electron micrographs of concentric circular grooves having a sinusoidal waveform cross section. Features are cut in 6061 aluminum using a microgrooving tool.

Fig. 7. Scanning electron micrographs of a micromachined 6061-T6 Al cylinder. Groove is 13.2-μm wide and 4-μm deep.

tently 13.1-μm wide over the entire cylinder length and nearly the same as the tool width, 13.0 μm. In addition, Fig. 8.b indicates a uniform 6° taper throughout the groove bottom, closely matching the shape of the tool end. Optical interferometry indicates that the roughness in the bottom of machined grooves remains small, similar to that for aluminum. By analyzing a number of line scans across segments of the micromachined groove, the average rms roughness is measured to be 0.25 μm.

Analysis of FIB-fabricated microtools immediately after machining cylindrical workpieces reveals that chips are cut and raked away from workpiece surfaces. An indication of this is shown in Fig. 9.a, which displays a long PMMA chip wrapped around the shank of a microtool. Note, the chip width is approximately equal to the cutting edge width. Additional SEM at higher magnification indicates chip raking. Fig. 9.b shows aluminum chips deflected by a rake facet with minimal accumulation behind the tool-end cutting edge.

5. Summary

This work successfully extends conventional shaping techniques to the microscale to fabricate curvilinear fea-
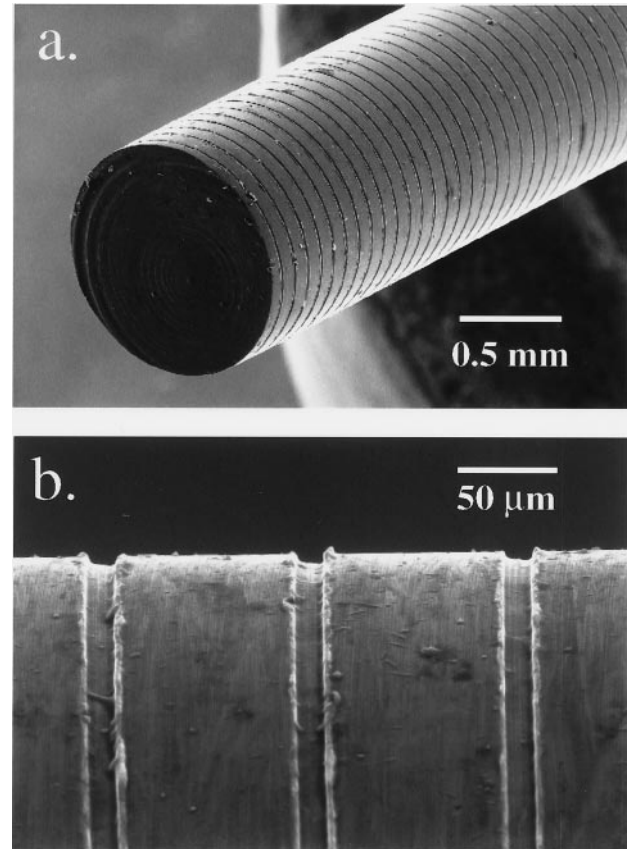
tures. Focused ion beam sputtering is used to fabricate microgrooving and microthreading tools that have well-defined back and side rake angles, cutting edge widths, and clearance tapers. Tools have cutting edge radii of curvature equal to 0.4 μm, although sharper edges may be possible with other tool materials. Focused ion beam tool fabrication has the advantage that almost any conceivable tool geometry can be fabricated on a scale that is well below those reached by grinding methods. In addition, this study demonstrates several examples of complex micromachined features, including sinusoidal cross-sectional features in planar samples and helices in cylindrical workpieces. Feature cross sections closely match tool shape when machining PMMA and aluminum alloy. These results suggest that other microtools; for example, those having nonorthogonal cutting edges, can accurately fabricate beveled grooves with a given desired cross section. Planing tests reveal that feature widths best match microgrooving tool widths for certain machining parameters. In addition, grooves in Al and brass have roughnesses, R_a, of approximately 0.12–0.30 μm. Further process improvements are considered possible.

Future work will combine this technique with other microfabrication processes, including thin film vapor deposition, electroplating, and hot embossing. Ultraprecision machining of thin films/coatings [32] will be explored to
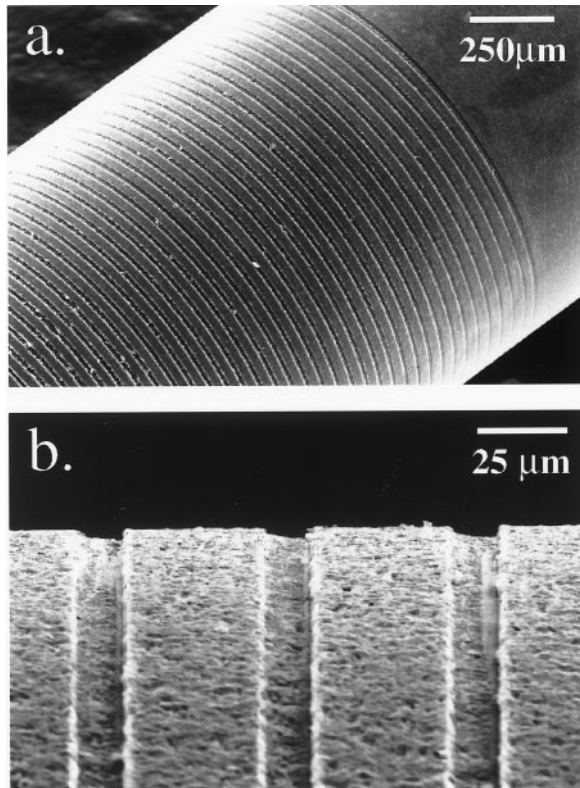
Fig. 8. Scanning electron micrographs of a micromachined PMMA cylinder. Groove is 13.1-μm wide and 4-μm deep.
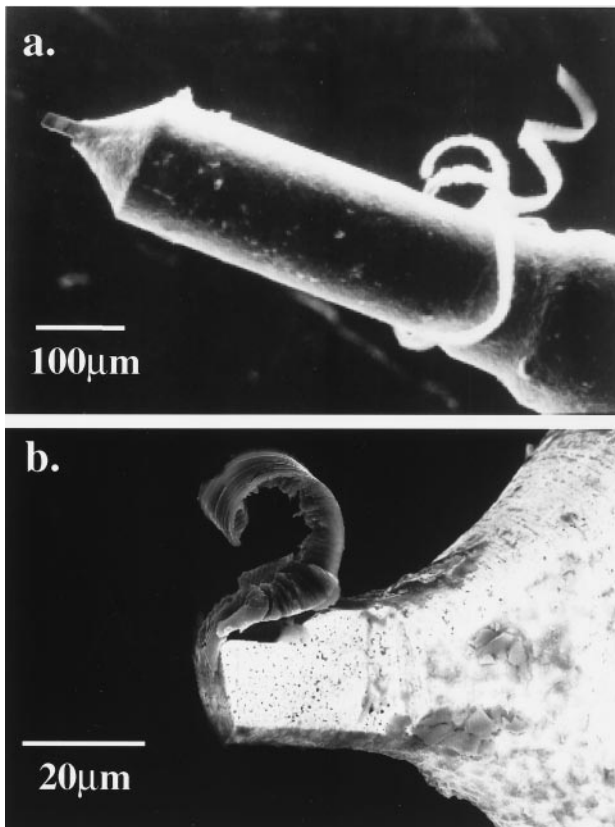

Fig. 9. Scanning electron micrographs of microgrooving tools immediately after machining PMMA (a.) and 6061-T6 aluminum (b.).

determine the influence of film microstructure and adhesion on micromachined feature quality.

References

[1] Thornell G, Johansson S. Microprocessing at the fingertips. J Micromech Microeng 1998;8:251–62.

[2] Webb AG. Radiofrequency microcoils in magnetic resonance. Prog Nucl Magn Reson Spectrosc 1997;31:1–42.

[3] Rogers JA, Jackman RJ, Whitesides GM. Constructing single- and multiple-helical microcoils and characterizing their performance as components of microinductors and microelectromagnets. J Microelectromech Syst 1997;6(3):184–92.

[4] Wagner B, Benecke W, Engelmann G, Simon J. Microactuators with moving magnets for linear, torsional, or multiaxial motion. Sens Actuators A 1992; 32:598–603.

[5] Jackman RJ, Brittain ST, Adams A, Prentiss MG, Whitesides GM. Design and fabrication of topologically complex, three-dimensional microstructures. Science 1998;280:2089–91.

[6] Lehmann O, Stuke M. Laser-driven movement of three-dimensional microstructures generated by laser rapid prototyping. Science 1995; 270:1644–46.

[7] Maxwell J, Larsson K, Boman M, Hooge P, Williams K, Coane P. Rapid prototyping of functional three-dimensional microsolenoids and electromagnets by high-pressure laser chemical vapor deposition. Proceedings of Solid Freeform Fabrication Symposium 1998;529–36.

[8] Becker EW, Ehrfeld W, Hagmann P, Maner A, Münchmeyer D. Fabrication of microstructures with high aspect ratios and great structural heights by synchrotron radiation lithography, galvano-forming, and plastic moulding (LIGA process). Microelectron Eng 1986;4:35–56.

[9] Christenson TR. Advances in LIGA-based postmold fabrication. Proc SPIE Micromach Microfabric Proc Technol IV 1998;3511:192–203.

[10] Schrempel F, Witthuhn W. Deep light ion lithography in PMMA—A parameter study. Nucl Instr Meth B 1997;132:430–38.

[11] Springham SV, Osipowicz T, Sanchez JL, Gan LH, Watt F. Micromachining using deep ion-beam lithography. Nucl Instr Meth B 1997;130:155–9.

[12] Feinerman AD, Lajos RE, White V, Denton DD. X-ray lathe: An x-ray lithographic exposure tool for nonplanar objects. J Microelectromech Syst 1996; 5(4):250–5.

[13] Liu RH, Vasile MJ, Beebe DJ. The fabrication of nonplanar spin-on glass microstructures. J Microelectromech Syst 1999;8(2):146–51.

[14] Ehrfeld W, Lehr H, Michel F, Wolf A, Gruber H-P, Bertholds A. Micro electro discharge machining as a technology in microma-

chining. Proc SPIE Micromac Microfabrica Symp 1996;2879: 332–7.

[15] Ehrfeld W, Hessel V, Lowe H, Schulz C, Weber L. Materials of LIGA technology. Microsyst Technol 1999;5(3):105–112.

[16] Orloff J. High-resolution focused ion beams. Rev Sci Instrum 1993; 64: 1105–30.

[17] Vasile MJ, Nassar R, Niu Z, Zhang W, Liu S. Focused ion beam milling: Depth control for three-dimensional microfabrication. J Vac Sci Technol B 1997; 15:2350.

[18] Ishitani T, Ohnishi T, Kawanami Y. Micromachining and device transplantation using focused ion beam. Japan J Appl Phys 1990;29: 2283–7.

[19] Vasile MJ, Biddick CJ, Schwalm SA. Microfabrication by ion milling: The lathe technique. J Vac Sci Technol B 1994;12:2388.

[20] Russell PE, Stark TJ, Griffis DP, Phillips JR, Jarausch KF. Chemically and geometrically enhanced focused ion-beam micromachining. J Vac Sci Technol B 1998;16:2494–8.

[21] Masuzawa T, Fujino M. A process for manufacturing very fine pin tools. SME Technical Papers MS90-307, 1990.

[22] Schaller Th, Bohn L, Mayer J, Schuber K. Microstructure grooves with a width of less that 50 μm cut with ground hard metal micro end mills. J Prec Eng 1999;23:229–35.

[23] Vasile MJ, Friedrich CR, Kikkeri B, McElhannon R. Micrometer-scale machining: Tool fabrication and initial results. J Prec Eng 1996;19(2/3):180–6.

[24] Friedrich CR, Vasile MJ. Development of the micromilling process for high aspect ratio microstructures. J Microelectromech Syst 1996; 5:33.

[25] Adams DP, Benavides G, Vasile MJ. Micrometer-scale machining of metals and polymers enabled by focused ion beam sputtering. Mat Res Soc Proc 1999; 546:201–6.

[26] Adams DP, Vasile MJ, Benavides G, Campbell A. Micromilling of metal alloys with focused ion beam-fabricated tools. submitted for publication 2000.

[27] Sigmund P. In: Inelastic Ion-Surface Collisions. Tolk N, et al., eds. New York: Academic Press, pp. 121–52, 1977.

[28] Sigmund P. In: Sputtering by Particle Bombardment, I. Behrisch R, ed. New York: Springer-Verlag, Ch. 2, 1981.

[29] Ochiai Y, Gamo K, Namba S. Pressure and irradiation angle dependence of maskless ion-beam assisted etching of GaAs and Si. J Vac Sci Technol B 1985; 3: 67–70.

[30] Harriott LR. A second generation focused ion beam micromachining system. Proc SPIE 1987;773:190.

[31] Vasile MJ, Nassar R, Xie J, Guo H. Microfabrication techniques using focused ion beams and emergent applications. Micron 1999; 30:235–44.

[32] Friedrich C, Coane P, Goettert J, Gopinathin N. Direct fabrication of deep x-ray lithography masks by micromechanical milling. J Prec Eng 1999;22: 164–73.